THE JOURNAL OF PHYSICAL CHEMISTRY B

Article

pubs.acs.org/JPCB

Long-Lived Intermediates in a Cooperative Two-State Folding Transition

Tarick J. El-Baba,[†] Doyong Kim,[‡] Dylan B. Rogers,[§] Faizan A. Khan,[§] David A. Hales,[§] David H. Russell,[‡] and David E. Clemmer*[,†]

[†]Department of Chemistry, Indiana University, 800 Kirkwood Avenue, Bloomington, Indiana 47401, United States

[‡]Department of Chemistry, Texas A&M University, College Station, Texas 77843, United States

[§]Department of Chemistry, Hendrix College, Conway, Arkansas 72032, United States

Supporting Information

ABSTRACT: Biomolecular folding often occurs through a *cooperative* two-state *reactant* ↔ *product* transition; the term *cooperative* does not convey that intermediate structures are nonexistent but rather that these states are not observable by existing experimental techniques. Because of this, few intermediates have been studied and characterized. Recently, ion mobility spectrometry (IMS) measurements revealed that the oligomer polyproline-13 (Pro13, which in propanol (PrOH) favors the right-handed helical PPI structure having adjacent pyrrolidine rings in a *cis* configuration) folds through six sequential long-lived intermediates as it converts to the all-*trans*-configured PPII structure that is favored in aqueous solutions. Here, we examine the PPI_{PrOH} → $PPII_{aq}$ folding transition for a HisPro13 sequence, i.e., Pro13 having a single histidine residue added to the N-terminus. Remarkably, the IMS measurements show that, upon addition of histidine, all of the IMS peaks associated with intermediate structures disappear. Instead, HisPro13 folds via a cooperative two-state transition, delayed by a significant induction period. The induction period is temperature dependent—shifting the transition to longer times at lower temperatures. Equilibrium studies show that the HisPro13 PPI_{PrOH} → $PPII_{aq}$ transition is endothermic but favored entropically. From these clues, we propose a sequential folding mechanism and develop a model that suggests that ∼13−17 long-lived intermediates are likely responsible for the induction period. In this model, intermediates are separated by average individual activation barriers of ∼90 kJ·mol^{-1}, and are entropically favorable.

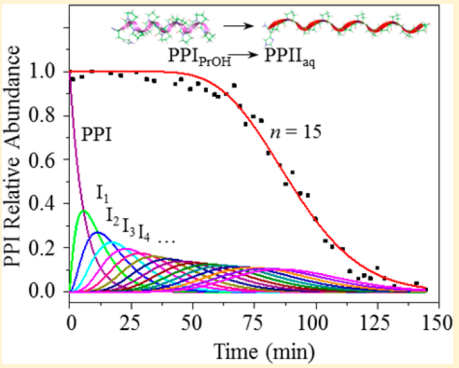

INTRODUCTION

Macromolecular folding is generally conceived as a *cooperative* two-state process involving only the unfolded and folded structures.[1−3] Such transitions are believed to occur through intermediate states along pathways that guide folding.[4] While computational models are valuable for understanding folding,[5−10] it is rare that intermediate states are captured experimentally.[11−13] Thus, comparisons between theoretical and experimental measurements are rare, at least in part because traditional experimental techniques are not particularly sensitive to intermediate states—presumably because ensembles of many different structures are present simultaneously. New techniques that can isolate and characterize structures of systems that display multiple intermediates would make it possible to rigorously test theoretical models and aid in structure prediction.[4,14−16]

A number of groups are now using electrospray ionization (ESI)[17] coupled with ion mobility spectrometry (IMS) and mass spectrometry (MS) methods to characterize ion structures and correlate these structures with conformations that exist in solution.[18−27] In favorable cases, the evaporative cooling phenomenon associated with a drying droplet appears to trap metastable structures as they transition into the gas phase.[25,28,29] IMS can rapidly separate different configurations (on ms time scales) based on differences in their mobilities through an inert buffer gas.[30,31] Thus, the combination of techniques makes it possible to resolve species from solution that in some cases cannot be observed with any other existing technology.[19,21,22,26,27,32]

Polyproline is a system that has attracted considerable attention since the 1950s.[33] These oligomers adopt helical structures that are influenced by their environment: when incubated in propanol, polyproline forms a well-defined right-handed polyproline I (PPI) helix, in which adjacent pyrrolidine rings are configured in a *cis* orientation; immersion in aqueous solutions causes the PPI helix to spontaneously flip every peptide bond in order to produce an all-*trans* polyproline II (PPII) helical form.[34−36] Recent IMS studies revealed the presence of at least six, long-lived folding intermediates involved in the solvent-induced PPI_{PrOH} → $PPII_{aq}$ transition

Received: September 4, 2016
Revised: November 1, 2016
Published: November 5, 2016

DOI: 10.1021/acs.jpcb.6b08932
J. Phys. Chem. B 2016, 120, 12040−12046

for a 13-residue polyproline oligomer (Pro13). Kinetics studies show that this transition proceeds through a mechanism in which adjacent peptide bonds are sequentially reoriented beginning from the N-terminus of the peptide.[26,27] For Pro13, which has 12 peptide bonds, there are 479,001,600 (12!) direct *cis* → *trans* folding pathways between the PPI and PPII helical forms. Remarkably, all of the experimental intermediates appear to fall along a single pathway. Studies as a function of solution temperature provided thermodynamic insight about how and why the transition occurs.[26,27]

In the present study, we extend this work to a 14-residue polypeptide histidine-Pro13 (HisPro13, see Scheme 1) and find that, in this system, the $PPI_{PrOH} \rightarrow PPII_{aq}$ transition proceeds on a time scale that is similar to Pro13; however, no IMS peaks, associated with intermediate structures, are detected. Instead, the transition occurs via a cooperative two-state transition after a well-defined induction period. Studies of this transition as a function of solution temperature show that the transition time associated with the induction period is strongly temperature dependent. Below, we describe these measurements and develop a model to explain these observations. It appears that, while IMS peaks associated with the Pro13 intermediates are not detected, intermediates likely do exist and thus are responsible for the induction period. From our analysis, we are able to capture insight about the number of intermediate states as well as the average nature of the folding landscape without directly detecting these intermediates.

Scheme 1. Representative Ideal Structure for the (a) PPI and (b) PPII Helices of HisPro13[a]

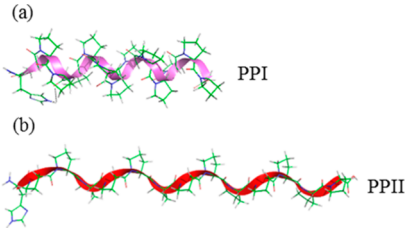

[a]Helical ribbons trace the backbone to illustrate the different helix lengths. Dihedral angles are (a) $\Phi = 74°$, $\Psi = 130°$, and $\omega = -11°$ for His^1-Pro^2 and $\Phi = -83°$, $\Psi = 158°$, and $\omega = 0°$ for the Pro-Pro bonds and (b) $\Phi = -78°$, $\Psi = 149°$, and $\omega = 180°$. See ref 57.

The present work is related to other systems where proline regulates folding—particularly dynamic structural regions.[37] The His-Pro moiety, which is found in regions associated with signaling and regulatory processes,[38−42] is known to be sensitive to temperature and pH,[43] an outcome of the aromatic and basic nature of the imidazole ring.[44−46] Systematic studies of how amino acids at different locations in these oligomers may reveal more details about how and why specific transitions occur. We begin such studies with HisPro13 primarily because we anticipate that the histidine will be protonated (under our solution conditions) and thus should stabilize the helical macrodipole[47] (and thus influence the folding mechanism).

EXPERIMENTAL SECTION

Peptide Synthesis. All synthesis reagents were purchased from Midwest Biotech (Indianapolis, IN), except for 3-(diethoxy-phosphoryloxy)-3*H*-benzo[*d*][1,2,3]-triazin-4-one, which was purchased from Aapptec (Louisville, KY). All solvents used were of the highest purity. HisPro13 was synthesized using a modified Applied Biosystems 430A synthesizer (Applied Biosystems, Foster City, CA) by the standard Boc solid-phase synthesis protocol, which has been described in detail previously.[26]

Sample Preparation. The HisPro13 peptide was dissolved in pure 1-propanol (PrOH) to a concentration of ∼160 μM and incubated at room temperature for at least 72 h to ensure the initial equilibrium distribution was reached. The PPI → PPII transition was initiated by dilution of the PrOH stock solution to ∼16 μM with H_2O and acetic acid (HOAc) to a final solution composition of 10:88:2 PrOH/H_2O/HOAc. The transition was followed at five temperatures (298, 303, 308, 313, and 318 K). Each temperature was defined by incubating the diluted sample solution in an appropriate water bath for 24 h prior to initiating the transition. At specific times after the transition was induced, sample aliquots were deposited into a sample tray held at 277 K and introduced into an electrospray needle tip for immediate analysis. After the transition appeared to be complete, solutions continued to be incubated and sampled periodically for ∼4−6 more h to ensure the final equilibrium distribution was reached.

General. IMS-MS instrumentation[48,49] and theory[50−53] are described in detail elsewhere. Experiments here were performed on a home-built IMS-time-of-flight instrument which is capable of IMS-IMS experiments. Briefly, mobility measurements are carried out as follows. Ions generated by nano-ESI (TriVersa NanoMate autosampler, Advion, Ithaca, NY) are trapped in an hourglass-shaped ion funnel[54] and are periodically released (150 μs per pulse) by an electrostatic shutter into an ∼1.8 m drift tube filled with ∼3.0 ± 0.03 Torr He. The ions are separated on the basis of their differences in mobility as they travel through the drift tube under the influence of a weak electric field (10 $V \cdot cm^{-1}$) while moving through the inert He buffer gas. Upon exiting the drift tube, ions are pulsed into an orthogonal time-of-flight mass spectrometer for mass-to-charge (m/z) separation and detected using a microchannel plate detector. The short acquisition time of time-of-flight mass spectrometry allows the IMS-MS data to be collected and represented in a nested drift time (m/z) fashion.[55]

Determination of Experimental Collision Cross Section. Measured ion mobility distributions are expressed as the experimentally measured drift time (t_D). The drift time can be converted into an ion-neutral collision cross section (Ω) using eq 1[50]

$$\Omega = \frac{(18\pi)^{1/2}}{16}\frac{ze}{(k_b T)^{1/2}}\left[\frac{1}{m_I}+\frac{1}{m_B}\right]^{1/2}\frac{t_D E}{L}\frac{760}{P}\frac{T}{273.2}\frac{1}{N} \quad (1)$$

where ze is the charge on the ion, k_b is the Boltzmann constant, T is the absolute temperature of the buffer gas, and m_I and m_B are the respective masses of the ion and He buffer gas. The values E, L, P, and N are the applied electric field, the length of the drift tube, the pressure of the buffer gas, and the neutral number density of the buffer gas (at STP), respectively.

Analysis of Experimental Data. Ion mobility data were collected at different time points along the $PPI_{PrOH} \rightarrow PPII_{aq}$ transition at all five temperatures. As described previously,[27] the relative abundance of each conformer as a function of transition time was determined for each timestamped spectrum using the peak analyzer tool in Origin version 9.2.2 (OriginLab Corporation, Northampton, MA).

DOI: 10.1021/acs.jpcb.6b08932
J. Phys. Chem. B 2016, 120, 12040−12046

In the work presented here, a kinetic model was developed to fit the induction period prior to the two-state cooperative transition. This model includes a series of intermediates that are not individually observed in the experiment but which cause an induction period such as that observed experimentally. A series of differential rate expressions were solved, one for each assumed change of conformation. The expressions for all of the steps were summed to yield an expression for the overall consumption of the PPI conformation. The resulting equation, which expresses the total abundance at a specific time point as a linear combination of n intermediates, is solved numerically across the abundance profile based on the best fit to the rate constant k. The rate constants were determined by allowing the fitting program to optimize the parameters for a maximum of 6.0×10^6 iterations, providing an analytical solution which was compared to the experimental data. The total abundance of the HisPro13 PPI conformation, for a sequential mechanism with n assumed intermediates, can be expressed by eq 2

$$f(t, n) = \sum_{1}^{n} \frac{1}{n!}(kt)^n e^{(-k \cdot t)} \quad (2)$$

where k is the rate constant (in s^{-1}), t is the time (in s), and n is the number of intermediate conformations. To determine the goodness of the fitting, the residual sum of squares was taken as an average over triplicate trials at each temperature and then summed over all temperatures to obtain a sum of the residual sum of squares (ΣRSS).

Molecular Dynamics Simulations and Cross Section Calculations. Molecular dynamics simulations were conducted on a Linux workstation using the Insight II 2005 simulation software (Accelrys Inc., San Diego, CA). The two protons were positioned at the N-terminus and His[1] side chain, respectively, based on pK_a and gas-phase basicity values reported previously.[56] The initial Pro-Pro dihedral angles were set to the optimum values for PPI and PPII helices.[57] The initial His-Pro dihedral angles were determined to have little effect on the calculated cross sections (see the Supporting Information). Energy minimization was carried out using the Discover_3 module with the extensible systematic force field. Simulations were conducted by placing the initial conformation in an environment with a dielectric constant of 1.0 at 300 K and allowing the structure to relax to its lowest energy conformation over 2 ns with a 20 ps step size. Calculated collision cross sections (Ω_{calc}) determined by the trajectory method using MOBCAL[52] (Indiana University, Bloomington, IN) were deemed candidate structures for specific IMS peaks when Ω_{calc} for the model structure was within ±2% of the experimental cross section (Ω_{expt}).

RESULTS AND DISCUSSION

Experimental Cross Section Distributions Showing the Time Dependence of $PPI_{PrOH} \rightarrow PPII_{aq}$ Transition. Figure 1 shows the collision cross section distributions at 298 and 318 K at several representative time points along the $PPI_{PrOH} \rightarrow PPII_{aq}$ transition. First, we consider the 298 K data set. Prior to initiating folding, a single peak, corresponding to a $[M + 2H]^{2+}$ form of the HisPro13 oligomer, is observed in the IMS-MS distribution. This peak is centered at $\Omega = 330$ Å^2 and corresponds to the helical PPI form of the doubly protonated HisPro13 oligomer ($\Omega_{calc} = 331 \pm 4$ Å^2). The $PPI_{PrOH} \rightarrow PPII_{aq}$ transition was induced upon addition of water to the oligomer in propanol stock solution to a final solution composition of

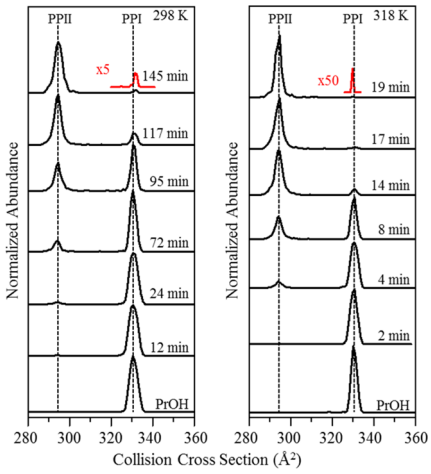

Figure 1. Collision cross section distribution for the $[M + 2H]^{2+}$ ions of HisPro13 collected during different times along the transition from $PPI_{PrOH} \rightarrow PPII_{aq}$ at (left) 298 K and (right) 318 K. Dashed lines delineate the positions for the PPI ($\Omega = 330$ Å^2) and PPII ($\Omega = 294$ Å^2) conformations.

10:88:2 PrOH:H_2O:HOAc. Immediately upon preparing this solution, there is no noticeable change in the distribution. After ~72 min, a new peak associated with a more compact (higher mobility) conformation appearing at $\Omega = 294$ Å^2 is observed. This ion is favored upon incubation of the oligomer in an aqueous solution and as shown below is consistent with the PPII configuration of the oligomer that is present in solution ($\Omega_{calc} = 291 \pm 5$ Å^2). As is the case for the PPII from Pro13, when the HisPro13 PPII helix is introduced into the gas phase as the solvent-free $[M + 2H]^{2+}$ species, the extended PPII helical structure (as shown in Scheme 1) collapses to self-solvate the charged sites on the ion, which results in an experimental cross section that is significantly smaller than expected for the PPII helix.[26] Over time in solution, the abundance of this peak increases while the signal for the PPI conformer drops, indicating that the new structure is a product of the PPI precursor. After 145 min, the distributions remain unchanged, an indication that the system has reached equilibrium. It is important to note that, unlike the Pro13 system, at 298 K, there is no direct evidence in the IMS distributions for any peaks other than the precursor PPI and product PPII structures. Thus, addition of the single His residue to Pro13 effectively removes all of the intermediate states observed for Pro13.

Figure 1 also shows data obtained while maintaining transition at 318 K. These data (as well as those recorded at other temperatures) are qualitatively similar to the 298 K measurements. That is, the cross section distributions are initially dominated by the peak centered at $\Omega = 330$ Å^2. This peak dominates the distribution for ~8 min after initiating the $PPI_{PrOH} \rightarrow PPII_{aq}$ transition. At longer times, the abundance of the compact conformation accumulates and ultimately becomes the dominant population. This transition is also absent of intermediates, and reaches equilibrium after ~19 min.

Unusual Kinetics along the $PPI_{PrOH} \rightarrow PPII_{aq}$ Transition for His-Pro13. Figure 2 shows the relative intensities of the two experimental peaks over time. At 298 K, the PPI peak persists with only a small loss of intensity until ~60 min; at this time, the PPI signal decays and there is a corresponding increase in intensity of the PPII signal. At higher solution temperatures, there is no immediate change in the relative

DOI: 10.1021/acs.jpcb.6b08932
J. Phys. Chem. B 2016, 120, 12040−12046

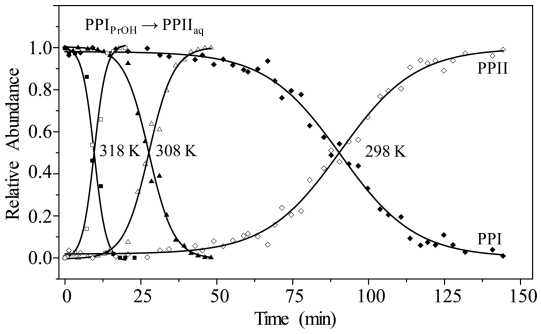

Figure 2. Kinetics plots of the PPI (filled points) to PPII (open points) transition at 318 K (squares), 308 K (triangles), and 298 K (diamonds) for the $PPI_{PrOH} \rightarrow PPII_{aq}$ transition. Lines are shown to guide the eye through the transition at each temperature.

abundance of the PPI conformation; instead, transitions are delayed by ~12 and 4 min at 308 and 318 K, respectively. This behavior is very different from the single exponential decay expected for a unimolecular transition.[58] In terms of precursor PPI loss and product accumulation, this system appears similar to the overall transition observed for Pro13. That is, the abundances of the PPI precursor and PPII final product are each relatively stable until a substantial induction period has passed. In Pro13, the origin of the delay is clear; in the intermediate states, which are observed directly as new IMS peaks, rise and fall in abundance during the induction period is associated with the loss and formation of reactants and products, respectively. The overall similarities of the HisPro13 system and Pro13 system suggest that the transition of HisPro13 also folds through intermediate states but that these are not observable by ESI-IMS-MS measurements.

Equilibrium Thermochemistry. While the measured kinetics are somewhat complex, once the transition is completed, it is straightforward to determine temperature-dependent equilibrium constants for this system. Figure 3

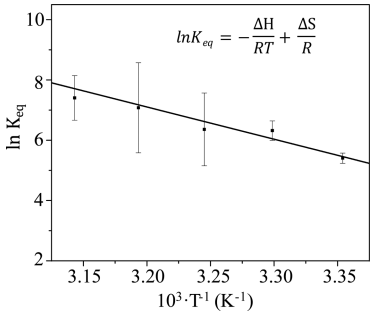

Figure 3. van't Hoff plot of ln K_{eq} versus the inverse temperature of the $PPI_{PrOH} \rightarrow PPII_{aq}$. Error bars represent the standard deviation of triplicate measurements. Calculated equilibrium thermochemistry: $\Delta G = -14 \pm 35$ kJ·mol^{-1}, $\Delta H = 72 \pm 12$ kJ·mol^{-1}, $\Delta S = 300 \pm 81$ J·mol^{-1}·K^{-1}.

shows a van't Hoff plot of these data, from which we determine the experimental thermochemistry for HisPro13 in water: $\Delta G = -14 \pm 35$ kJ·mol^{-1}, $\Delta H = 72 \pm 12$ kJ·mol^{-1}, and $\Delta S = 300 \pm 81$ J·mol^{-1}·K^{-1}. Thus, for HisPro13, the $PPI_{PrOH} \rightarrow PPII_{aq}$ is endothermic, driven by the increase in entropy of the system. This result is similar to the equilibrium thermochemistry observed for the PPI and PPII structures for the His-free Pro13 oligomer—$\Delta G = -18 \pm 13$ kJ·mol^{-1}, $\Delta H = 21 \pm 9$ kJ·mol^{-1}, and $\Delta S = 130 \pm 30$ J·mol^{-1}·K^{-1}—although the magnitudes of these values are greater for the HisPro13 system.[27]

Kinetics Models for a Two-State Transition. The observed induction period for the HisPro13 system, and similarities in overall time scales and thermochemistry of this system with Pro13 (where intermediates were directly measured), encourages us to develop a model for the HisPro13 system that assumes that intermediates (although not observed directly) may still play a role in the observed induction period. After extensive consideration of many possibilities, we propose a simple model based on sequential unimolecular kinetics to account for the induction period. The simplest sequential model through which a discrete number of intermediates (n) share a common rate constant is shown on the left column in Figure 4 for the decay of the PPI conformer at 298 K. By

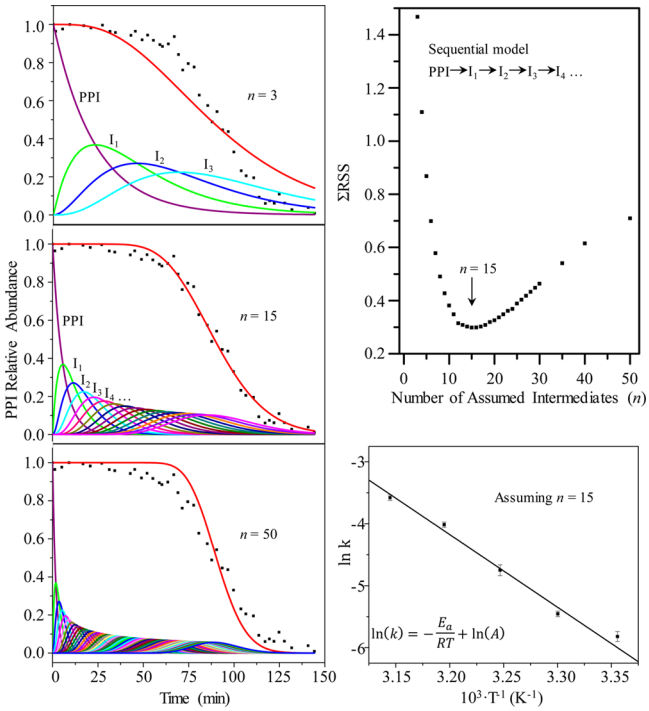

Figure 4. Sequential models for the $PPI_{PrOH} \rightarrow PPII_{aq}$ at 298 K involving 3 intermediates (left column, top), 15 intermediates (left column, middle), and 50 intermediates (left column, bottom). Filled points represent experimental data, red lines show the best fit, and colored lines represent intermediate conformations. Total residual sum of squares plotted against the number of assumed intermediates (n) for an entirely sequential model for the transition from $PPI_{PrOH} \rightarrow PPII_{aq}$ (right column, top). Minimum ΣRSS, and therefore the best fit, is found at $n = 15$. Arrhenius plot of ln k versus inverse temperature found using the $n = 15$ model. Error bars represent the standard deviation of triplicate measurements. Thermodynamic values at the transition state: $E_a = 93 \pm 3$ kJ·mol^{-1}, $\Delta G^{\ddagger} = 90 \pm 5$ kJ·mol^{-1}, $\Delta H = 92 \pm 5$ kJ·mol^{-1}, and $\Delta S = 11 \pm 4$ J·mol^{-1}·K^{-1}.

assuming that these intermediates exist and contribute to the total ion population, the induction period can be accounted for by summing the solutions to n number of differential rate expressions to produce an overall fitting curve which is optimized on the basis of the rate constant k (see eq 2).

The first fitting model assumes the PPI loss is followed by the growth and decay of only three intermediate species that are separated by the same activation barrier ($k_3 = 7.2 \pm 0.8 \times 10^{-4}$ s^{-1}) prior to formation of the PPII product (top panel).

DOI: 10.1021/acs.jpcb.6b08932
J. Phys. Chem. B 2016, 120, 12040−12046

By summing the overall abundances of each species (i.e., PPI, I_1, I_2, and I_3), an overall sigmoidal fitting curve is achieved. While this model produces a fit with the correct shape, it misses the experimental points. A good representation of the experimental data is found when we assume that 15 intermediate conformations contribute to the induction period (middle panel). In this model, the PPI conformation decays to the first intermediate, which sequentially propagates through 15 intermediates each at rate $k_{15} = 3.0 \pm 0.2 \times 10^{-3}$ s^{-1}, to eventually form the PPII product. The bottom plot in Figure 4 shows a model that assumes as many as 50 intermediates, each with rate constant $k_{50} = (9.1 \pm 0.6) \times 10^{-3}$ s^{-1}. This model, however, requires many rapidly decaying intermediates to account for the induction period, and the resulting fitting curve completely misses the experimental points. None of the other mechanisms that were considered (e.g., with varying rates, parallel mechanisms, etc., see the Supporting Information) represent the data as well as the entirely sequential processes with each step having the same rate constant. This includes fitting the experimental data to the mechanism proposed for the $PPI_{PrOH} \rightarrow PPII_{aq}$ transition for Pro13.[26]

The goodness of fit for the sequential model is shown in Figure 4, which plots the residual sum of squares (ΣRSS) against the number of intermediate conformations n. The best representation of the experimental data (where ΣRSS is at a minimum) is when $n = 15$ intermediates are assumed, which is strikingly close to the number of peptide bonds in a 14-residue polypeptide. Outside of the range $13 \leq n \leq 17$, the ΣRSS begins to increase dramatically, which indicates that these models provide unreasonable fits. The goodness of fit analyses for the other models that we have considered (seven different mechanisms in total, ranging from completely sequential to largely parallel) are presented in the Supporting Information. Those that have a faster or slower step in the procession of intermediates accurately capture the data when between 17 and 21 intermediates are considered, albeit with a much higher magnitude for the overall ΣRSS.

Figure 4 also shows the Arrhenius plot obtained by fitting $\ln(k)$ as a function of the inverse temperature, where rate constants were derived from the sequential fitting model where $n = 15$ (see above). The values extracted from this Arrhenius plot provide the averaged thermochemistry for each of the presumed transition states. We find $A = 10^{(13.9\pm0.6)}$ s^{-1} and $E_a = 93 \pm 3$ kJ·mol^{-1}. The latter value is similar to activation barriers measured for His-Pro moieties by Fischer and co-workers (103 ± 15 kJ·mol^{-1})[37,43] and also similar to values for each step for the Pro13 *cis*-to-*trans* isomerization (71−95 kJ·mol^{-1}).[26,27] As previously described, these values can be converted to the transition state values of $\Delta H^{\ddagger} = 92 \pm 5$ kJ·mol^{-1} and $\Delta S^{\ddagger} = 11 \pm 4$ J·mol^{-1}·K^{-1} for each of the $n = 15$ transitions; these can be combined to give the free-energy barrier of $\Delta G^{\ddagger} = 90 \pm 5$ kJ·mol^{-1} for each of the transition states. We find that, overall, the transition state thermochemistry is relatively insensitive to the number of intermediates. An estimate of the upper limit of $\Delta G^{\ddagger} = 91 \pm 3$ kJ·mol^{-1}, $\Delta H^{\ddagger} = 94 \pm 3$ kJ·mol^{-1}, and $\Delta S^{\ddagger} = 7 \pm 1$ J·mol^{-1}·K^{-1} to the thermochemical barriers can be obtained from the $n = 3$ model; an estimate of the lower limit of the barrier comes from the values derived from the $n = 50$ model: $\Delta G^{\ddagger} = 85 \pm 3$ kJ·mol^{-1}, $\Delta H^{\ddagger} = 91 \pm 3$ kJ·mol^{-1}, and $\Delta S^{\ddagger} = 23 \pm 2$ J·mol^{-1}·K^{-1}.

Why Are Intermediates Not Detected in HisPro13 $PPI_{PrOH} \rightarrow PPII_{aq}$? The dearth of intermediates might be explained by considering the relative stabilities for PPI and PPII for the Pro13 and HisPro13 structures. In order to understand these systems, we carried out rather extensive molecular modeling simulations, as we have done for many other peptide systems. In summary, we found no obvious differences between HisPro13 and Pro13, indicating that the level of theory that we applied was insensitive to the changes observed experimentally. Therefore, we limit this discussion to expected qualitative differences. In this system, the PPI structure contains a macrodipole oriented such that the negative pole is toward the N-terminus. Protonation on this side of the molecule will stabilize this dipole; because histidine is more basic than the backbone imide sites, we anticipate that the PPI form of HisPro13 will be relatively more stable than this form of Pro13. Such interactions are known to enhance helix stability, especially *in vacuo*.[59,60] The additional proton on the aromatic His side chain can facilitate hydrogen bonding interactions with neighboring amide carbonyls,[37,43] and rotomers of His can guide the His over α/δ-hydrogens on proximal Pro residues, forming π/CH overlap.[44−46] These interactions should stabilize the PPI precursor relative to the PPII product, which has little if any helix dipole and is stabilized by intermolecular solvent−solute interactions. Having noted this, we expect that the enhanced stability of the PPI helix comes at the cost of configurational entropy, as it limits this system to fewer accessible configurations, relative to the PPII structures.[61] Rather than *cis* → *trans* isomerization of individual peptide bonds, these data suggest the $PPI_{PrOH} \rightarrow PPII_{aq}$ transition begins by the PPI species ascending the free-energy barrier by hydration at the N-terminal charge sites followed by additional hydration along the peptide backbone. We expect that the intermediates formed in the $PPI_{PrOH} \rightarrow PPII_{aq}$ transition weaken the helix dipole as they are stabilized by solvent−molecule interactions. Removal of the lubricating solvent upon electrospraying the system into the gas phase may cause the less favorable intermediate structures to revert to the dipole-stabilized PPI structure. In this case, intermediates would not be observed as new peaks in the IMS distributions. As the transition proceeds, we expect a critical point in the transition is reached, and upon evaporation of the solvated intermediates, the PPII product is observed. That is, upon reaching the final PPII structure in solution, this system yields the PPII product without reverting to the PPI structure upon evaporation. In this way, the relative stability of the PPI helix for HisPro13 restricts the direct observation of intermediate states that were observed for Pro13. Higher-level theoretical studies, which can take into account changes in entropy at varying levels of solvation, may help clarify these observations.

CONCLUSIONS

The $PPI_{PrOH} \rightarrow PPII_{aq}$ transition for the HisPro13 peptide was investigated by ESI-IMS-MS techniques. Unlike Pro13, no peaks for intermediates are observed for HisPro13. Instead, the $PPI_{PrOH} \rightarrow PPII_{aq}$ HisPro13 transition proceeds rapidly, after a substantial induction period. The observation of a fast transition after such a long period of induction is remarkable and shows that the kinetics for the HisPro13 system does not follow typical unimolecular kinetics. To explain these systems, we postulated that intermediate conformations must exist for the HisPro13 in solution; however, the nature of these intermediates is such that they vanish upon introduction into the gas phase. This could be the case for a system where solvation to form intermediate states does not entirely change the peptide bond, such that upon desolvation the system can

DOI: 10.1021/acs.jpcb.6b08932
J. Phys. Chem. B 2016, 120, 12040−12046

recoil to produce the initial precursor PPI state. Presumably, the N-terminal addition of a His residue is responsible for this difference between the HisPro13 and Pro13 systems. Assuming that His remains protonated as the structural transition occurs, the presence of this residue might stabilize the macrodipole associated with the PPI state upon desolvation. In this way, the initial precursor state is apparently favored until the last peptide bond undergoes its *cis* → *trans* transition resulting in the PPII state. Analysis of the data leads us to propose a simple sequential model involving ∼13−17 intermdiates. The analysis provides the following insight about average thermochemical values, the transitions, and intermediates: $\Delta H^{\ddagger}$ = 92 ± 5 kJ·mol^{-1}, $\Delta S^{\ddagger}$ = 11 ± 4 J·mol^{-1}·K^{-1}, $\Delta G^{\ddagger}$ = 90 ± 5 kJ·mol^{-1}, ΔG = −14 ± 35 kJ·mol^{-1}, ΔH = 72 ± 12 kJ·mol^{-1}, and ΔS = 300 ± 81 J·mol^{-1}·K^{-1}. These data show that in some systems it is possible to determine the numbers and stabilities of key intermediates even when they are not directly observed as direct experimental signals—providing insight about the details of unobservable phenomena in two-state cooperative transitions.

■ ASSOCIATED CONTENT

Supporting Information

The Supporting Information is available free of charge on the ACS Publications website at DOI: 10.1021/acs.jpcb.6b08932.

Table of computed collision cross sections from gas-phase MD (Table S1); list of rate constants for each number of assumed intermediates for the model (Table S2); stacked cross section distributions at 303, 308, and 313 K at representative time points (Figure S1); kinetics plots of conformer abundance versus time at 303 and 313 K (Figure S2); other kinetics models evaluated for fitting of induction period in PPI decay (Figures S3−S5); plot of ΣRSS versus number of assumed intermediates for various candidate models (Figure S6) (PDF)

■ AUTHOR INFORMATION

Corresponding Author

*E-mail: clemmer@indiana.edu.

Notes

The authors declare no competing financial interest.

■ ACKNOWLEDGMENTS

The authors are grateful of Liuqing Shi for her discussion of preliminary results. This work is supported by funds from the Waters Corporation, the National Institutes of Health R01 GM103725 (D.E.C.), The Shideler-Hough Endowment for Education in Chemistry at Hendrix College (D.A.H.), and U.S. Department of Energy, Office of Science, Basic Energy Sciences DE-FG02-04ER15520 (D.H.R.).

■ REFERENCES

(1) Jackson, S. E.; Fersht, A. R. Folding of Chymotrypsin Inhibitor 2. 1. Evidence for a Two-State Transition. *Biochemistry* **1991**, *30*, 10428−10435.

(2) Weikl, T. R.; Palassini, M.; Dill, K. A. Cooperativity in Two-State Protein Folding Kinetics. *Protein Sci.* **2004**, *13*, 822−829.

(3) Qiu, L.; Pabit, S. A.; Roitberg, A. E.; Hagen, S. J. Smaller and faster: the 20-residue Trp-Cage Protein Folds in 4 Microseconds. *J. Am. Chem. Soc.* **2002**, *124*, 12952−12953.

(4) Dill, K. A.; MacCallum, J. The Protein-Folding Problem, 50 Years On. *Science* **2012**, *338*, 1042−1046.

(5) Rollins, G. C.; Dill, K. A. General Mechanism for Two-State Protein Folding Kinetics. *J. Am. Chem. Soc.* **2014**, *136*, 11420−11427.

(6) Doig, A. J. Recent Advances in Helix-Coil Theory. *Biophys. Chem.* **2002**, *101−102*, 281−293.

(7) Lifson, S.; Roig, A. On the Theory of Helix-Coil Transition in Polypeptides. J. *J. Chem. Phys.* **1961**, *34*, 1963−1974.

(8) Chan, H. S.; Bromberg, A.; Dill, K. A. Models of Cooperativity in Protein Folding. *Philos. Trans. R. Soc., B* **1995**, *348*, 61−70.

(9) Ivankov, D. N.; Finkelstein, A. V. Prediction of Protein Folding Rates from the Amino Acid Sequence-Predicted Secondary Structure. *Proc. Natl. Acad. Sci. U. S. A.* **2004**, *101*, 8942−8944.

(10) Piana, S.; Lindorff-Larsen, K.; Shaw, D. E. Protein Folding Kinetics and Thermodynamics from Atomistic Simulation. *Proc. Natl. Acad. Sci. U. S. A.* **2012**, *109*, 17845−17850.

(11) Merchant, K. A.; Best, R. B.; Louis, J. M.; Gopich, J. M.; Eaton, W. A. Characterizing the Unfolded States of Proteins Using Single-Molecule FRET Spectroscopy and Molecular Simulations. *Proc. Natl. Acad. Sci. U. S. A.* **2007**, *104*, 1528−1533.

(12) Oliva, F. Y.; Munoz, V. A. Simple Thermodynamic Test to Discriminate Between Two-State and Downhill Folding. *J. Am. Chem. Soc.* **2004**, *126*, 8596−8597.

(13) Rovo, P.; Farkas, V.; Hegyi, O.; Csikos-Szolomajer, O.; Toth, G. K.; Perczel, A. J. Cooperativity Network of Trp-Cage Miniproteins: Probing Salt-Bridges. *J. Pept. Sci.* **2011**, *17*, 610−619.

(14) Motlagh, H.; Toptygin, D.; Kaiser, C. M.; Hilser, V. J. Single-Molecule Chemo-Mechanical Spectroscopy Provides Structural Identity of Folding Intermediates. *Biophys. J.* **2016**, *110*, 1280−1290.

(15) Hu, W.; Kan, Z.; Mayne, L.; Englander, S. W. Cytochrome c Folds Through Foldon-Dependent Native-Like Intermediates in an Ordered Pathway. *Proc. Natl. Acad. Sci. U. S. A.* **2016**, *113*, 3809−3814.

(16) Neupane, K.; Foster, D. A. N.; Dee, D. R.; Yu, H.; Wang, F.; Woodside, M. T. Direct Observation of Transition Paths During the Folding of Proteins and Nucleic Acids. *Science* **2016**, *352*, 239−242.

(17) Fenn, J. B.; Mann, M.; Meng, C. K.; Wong, S. F.; Whitehouse, C. M. Electrospray Ionization for Mass Spectrometry of Large Biomolecules. *Science* **1989**, *246*, 64−71.

(18) Loo, J. A.; Edmonds, C. G.; Udseth, H. R.; Smith, R. D. Effect of Reducing Disulfide-Containing Proteins on Electrospray Ionization Mass Spectra. *Anal. Chem.* **1990**, *62*, 693−698.

(19) Ruotolo, B. T.; Giles, K.; Campuzano, I.; Sandercock, A. M.; Bateman, R. H.; Robinson, C. V. Evidence for Macromolecular Protein Rings in the Absence of Bulk Water. *Science* **2005**, *310*, 1658−1661.

(20) Ruotolo, B. T.; Robinson, C. V. Aspects of Native Proteins Are Retained in Vacuum. *Curr. Opin. Chem. Biol.* **2006**, *10*, 402−408.

(21) Pierson, N. A.; Chen, L.; Valentine, S. J.; Russell, D. H.; Clemmer, D. E. Number of Solution States of Bradykinin from Ion Mobility and Mass Spectrometry Measurements. *J. Am. Chem. Soc.* **2011**, *133*, 13810−13813.

(22) Pierson, N. A.; Chen, L.; Russell, D. H.; Clemmer, D. E. Cis-Trans Isomerizations of Proline Residues Are Key to Bradykinin Conformations. *J. Am. Chem. Soc.* **2013**, *135*, 3186−3192.

(23) Wyttenbach, T.; Pierson, N. A.; Clemmer, D. E.; Bowers, M. T. Ion Mobility Analysis of Molecular Dynamics. *Annu. Rev. Phys. Chem.* **2014**, *65*, 175−196.

(24) Lanucara, F.; Holman, S. W.; Gray, C. J.; Eyers, C. E. The Power of Ion Mobility-Mass Spectrometry for Structural Characterization and the Study of Conformational Dynamics. *Nat. Chem.* **2014**, *6*, 281−294.

(25) McAllister, R. G.; Metwally, H.; Sun, Y.; Konermann, L. J. Release of Native-like Gaseous Proteins from Electrospray Droplets via the Charged Residue Mechanism: Insights from Molecular Dynamics Simulations. *J. Am. Chem. Soc.* **2015**, *137*, 12667−12676.

(26) Shi, L.; Holliday, A. E.; Shi, H.; Zhu, F.; Ewing, M. A.; Russell, D. H.; Clemmer, D. E. Characterizing Intermediates along the Transition from Polyproline I to Polyproline II using Ion Mobility Spectrometry-Mass Spectrometry. *J. Am. Chem. Soc.* **2014**, *136*, 12702−12711.

(27) Shi, L.; Holliday, A. E.; Glover, M. S.; Ewing, M. A.; Russell, D. H.; Clemmer, D. E. Ion Mobility-Mass Spectrometry Reveals the

DOI: 10.1021/acs.jpcb.6b08932
J. Phys. Chem. B 2016, 120, 12040−12046

Energetics of Intermediates that Guide Polyproline Folding. *J. Am. Soc. Mass Spectrom.* **2016**, *27*, 22−30.
(28) Silveira, J. A.; Fort, K. L.; Pierson, N. A.; Clemmer, D. E.; Russell, D. H. From Solution to the Gas Phase: Stepwise Dehydration and Kinetic Trapping of Substance P Reveals the Origin of Peptide Conformations. *J. Am. Chem. Soc.* **2013**, *135*, 19147−19153.
(29) Fort, K. L.; Silveira, J. A.; Pierson, N. A.; Servage, K. A.; Clemmer, D. E.; Russell, D. H. From Solution to the Gas Phase: Factors That Influence Kinetic Trapping of Substance P in the Gas Phase. *J. Phys. Chem. B* **2014**, *118*, 14336−14344.
(30) Clemmer, D. E.; Jarrold, M. F. Ion Mobility Measurements and Their Applications to Clusters and Biomolecules. *J. Mass Spectrom.* **1997**, *32*, 577−592.
(31) Bohrer, B. C.; Merenbloom, S. I.; Koeniger, S. L.; Hilderbrand, A. E.; Clemmer, D. E. Biomolecule Analysis by Ion Mobility Spectrometry. *Annu. Rev. Anal. Chem.* **2008**, *1*, 293−327.
(32) Do, T. D.; Bowers, M. T. Amino Acid Metaclusters: Implications of Growth Trends on Peptide Self-Assembly and Structure. *Anal. Chem.* **2015**, *87*, 4245−4252.
(33) Kurtz, Z.; Berger, A.; Katchalski, E. Mutarotation of Poly-L-Proline. *Nature* **1956**, *178*, 1066−1067.
(34) Traub, W.; Shmueli, U. Structure of Poly-L-Proline I. *Nature* **1963**, *198*, 1165−1166.
(35) Swenson, C. A.; Formanek, R. J. Infrared Study of Poly-L-Proline in Aqueous Solution. *J. Phys. Chem.* **1967**, *71*, 4073−4077.
(36) Forsythe, K. H.; Hopfinger, A. J. The Influence of Solvent on the Secondary Structures of Poly(L-Alanine) and Poly(L-Proline). *Macromolecules* **1973**, *6*, 423−437.
(37) Reimer, U.; Scherer, G.; Drewello, M.; Kruber, S.; Schutkowski, M.; Fischer, G. Side-Chain Effects on Peptidyl-Prolyl Cis/Trans Isomerization. *J. Mol. Biol.* **1998**, *279*, 449−460.
(38) Unkefer, C. J.; Walker, R. D.; London, R. E. Hydrogen-1 and Carbon-13 Nuclear Magnetic Resonance Conformational Studies of the His-Pro Peptide Bond: Conformational Behavior of TRH. *Int. J. Pept. Protein Res.* **1983**, *22*, 582−589.
(39) DeLeon, K. Y.; Patel, A. P.; Kuczera, K.; Johnson, C. K.; Jas, G. S. Structure and Reorintational Dynamics of Angiotensin I and II: A Microscopic Physical Insight. *J. Biomol. Struct. Dyn.* **2012**, *29*, 1175−1194.
(40) Juarez, J. C.; Guan, X.; Shipulina, N. V.; Plunkett, M. L.; Parry, G. C.; Shaw, D. E.; Zhang, J. C.; Rabbani, S. A.; McCrae, K. R.; Mazar, A. P.; et al. Histidine-Proline-Rich Glycoprotein Has Potent Antiangiogenic Activity Mediated Through the Histidine-Proline-Rich Domain. *Cancer Res.* **2002**, *62*, 5344−5350.
(41) Vanwildemeersch, M.; Olsson, A. K.; Gottfridsson, E.; Claesson-Welsch, L.; Lindahl, U.; Spillmann, D. J. The Anti-Angiogenic His/Pro-Rich Fragment of Histidine-Rich Glycoprotein Binds to Endothelial Cell Heparan Sulfate in a Zn^{2+}-Dependent Manner. *J. Biol. Chem.* **2006**, *281*, 10298−10304.
(42) Ronca, F.; Raggi, A. Structure-Function Relationships in Mammalian Histidine-Proline-Rich Glycoprotein. *Biochimie* **2015**, *118*, 207−220.
(43) Reimer, U.; ElMokdad, N.; Schutkowski, M.; Fischer, G. Intramolecular Assistance of Cis/Trans Isomerization of the Histidine-Proline Moiety. *Biochemistry* **1997**, *36*, 13802−13808.
(44) Zondlo, N. J. Aromatic−Proline Interactions: Electronically Tunable CH/π Interactions. *Acc. Chem. Res.* **2013**, *46*, 1039−1049.
(45) Pandey, A. K.; Thomas, K. M.; Forbes, C. R.; Zondlo, N. J. Tunable Control of Polyproline Helix (PPII) Structure via Aromatic Electronic Effects: An Electronic Switch of Polyproline Helix. *Biochemistry* **2014**, *53*, 5307−5314.
(46) Zondlo, N. J.; Forbes, C. R.; Pandey, A. K.; Naduthambi, D.; Thomas, K. M. Tunable Control of Peptide Structure via Aromatic-Proline CH/pi Interactions and Proline Stereoelectronic Effects. *J. Pept. Sci.* **2012**, *18*, S41−S42.
(47) Kuemin, M.; Schweizer, S.; Ochsenfeld, C.; Wennemers, H. Effects of Terminal Functional Groups on the Stability of the Polyproline II Structure: A Combined Experimental and Theoretical Study. *J. Am. Chem. Soc.* **2009**, *131*, 15474−15482.
(48) Merenbloom, S. I.; Koeniger, S. L.; Valentine, S. J.; Plasencia, M. D.; Clemmer, D. E. IMS−IMS and IMS−IMS−IMS/MS for Separating Peptide and Protein Fragment Ions. *Anal. Chem.* **2006**, *78*, 2802−2809.
(49) Koeniger, S. L.; Merenbloom, S. I.; Valentine, S. J.; Jarrold, M. F.; Udseth, H.; Smith, R. D.; Clemmer, D. E. An IMS−IMS Analogue of MS−MS. *Anal. Chem.* **2006**, *78*, 4161−4174.
(50) Mason, E. A.; McDaniel, E. W. *Transport Properties of Ions in Gases*; Wiley: New York, 1988.
(51) Shvartsburg, A. A.; Jarrold, M. F. An Exact Hard-Spheres Scattering Model for the Mobilities of Polyatomic Ions. *Chem. Phys. Lett.* **1996**, *261*, 86−91.
(52) Mesleh, M. F.; Hunter, J. M.; Shvartsburg, A. A.; Schatz, G. C.; Jarrold, M. F. Structural Information from Ion Mobility Measurements: Effects of the Long Range Potential. *J. Phys. Chem.* **1996**, *100*, 16082−16086.
(53) Wyttenbach, T.; von Helden, G.; Batka, J. J.; Carlat, D.; Bowers, M. T. Effect of the Long-Range Potential on Ion Mobility Measurements. *J. Am. Soc. Mass Spectrom.* **1997**, *8*, 275−282.
(54) Tang, K.; Shvartsburg, A. A.; Lee, H.-N.; Prior, D. C.; Buschbach, M. A.; Li, F.; Tolmachev, A. V.; Anderson, G. A.; Smith, R. D. High-Sensitivity Ion Mobility Spectrometry/Mass Spectrometry Using Electrodynamic Ion Funnel Interfaces. *Anal. Chem.* **2005**, *77*, 3330−3339.
(55) Hoaglund, C. D.; Valentine, S. J.; Sporleder, C. R.; Reilly, J. P.; Clemmer, D. E. Three-Dimensional Ion Mobility/TOFMS Analysis of Electrosprayed Biomolecules. *Anal. Chem.* **1998**, *70*, 2236−2242.
(56) Bleiholder, C.; Suhai, S.; Paizs, B. Revising the proton affinity scale of the naturally occurring alpha-amino acids. *J. Am. Soc. Mass Spectrom.* **2006**, *17*, 1275−1281.
(57) IUPAC-IUB Commission on Biochemical Nomenclature. *Biochemistry* **1970**, *9*, 3471−3479.
(58) Marcus, R. A. Interaction of Theory and Experiment in Reaction Kinetics. In *Comprehensive Chemical Kinetics*; Compton, R. G., Hancock, G., Eds.; Elsevier B.V.: Amsterdam, The Netherlands, 1999; Vol. *37*, pp 1−33.
(59) Hudgins, R. R.; Ratner, M. A.; Jarrold, M. F. Design of Helices That Are Stable *in vacuo*. *J. Am. Chem. Soc.* **1998**, *120*, 12974−12975.
(60) Kohtani, M.; Jarrold, M. F. The Initial Step in the Hydration of Unsolvated Peptides: Water Molecule Adsorption on Alanine-Based Helices and Globules. *J. Am. Chem. Soc.* **2002**, *124*, 11148−11158.
(61) Jarrold, M. F. Helices and Sheets *in vacuo*. *Phys. Chem. Chem. Phys.* **2007**, *9*, 1659−1671.

DOI: 10.1021/acs.jpcb.6b08932
J. Phys. Chem. B 2016, 120, 12040−12046